

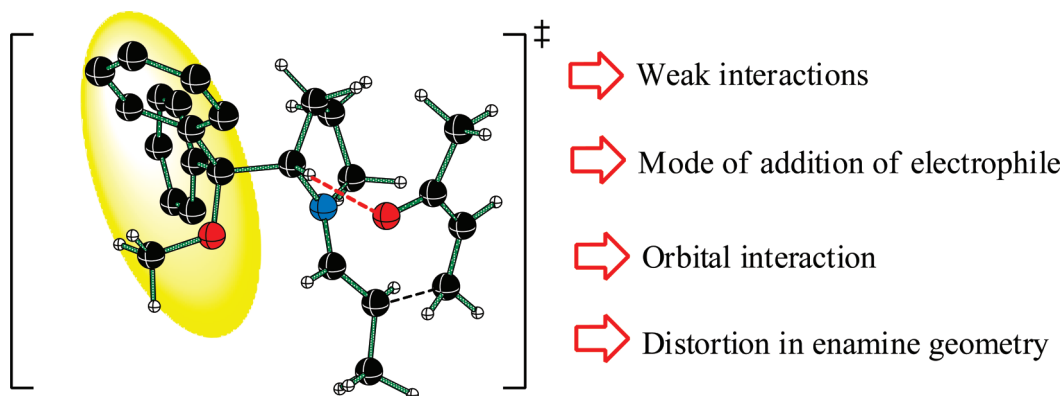
Importance of the Nature of α -Substituents in Pyrrolidine Organocatalysts in Asymmetric Michael Additions

Mahendra P. Patil, Akhilesh K. Sharma, and Raghavan B. Sunoj*

Department of Chemistry, Indian Institute of Technology Bombay, Powai, Mumbai 400076, India

sunoj@chem.iitb.ac.in

Received August 13, 2010



The fundamental factors contributing toward the stereoselectivity in organocatalyzed asymmetric Michael reaction between aldehydes (propanal and 3-phenyl propanal) and methyl vinyl ketone (MVK) are established by using density functional theory methods. Three of the most commonly employed α -substituted pyrrolidine organocatalysts are examined. Several key stereochemical modes of addition between (i) a model enamine or (ii) pyrrolidine enamines derived from aldehydes and secondary amine to MVK are examined. Among these possibilities, the addition of (*E*)-enamine to *cis*-MVK is found to have a lower activation barrier. The stereochemical outcome of the reaction is reported on the basis of the relative energies between pertinent diastereomeric transition states. Moderate selectivity is predicted for the reaction involving pyrrolidine catalysts **I** and **II**, which carry relatively less bulky α -substituents dimethylmethoxymethyl and diphenylmethyl, respectively. On the other hand, high selectivity is computed in the case of catalyst **III** having a sufficiently large α -substituent (diarylmethoxymethyl or diphenylprolinol methyl ether). The enantiomeric excess in the case of 3-phenyl propanal is found to be much higher as compared to that with unsubstituted propanal, suggesting potential for improvement in stereoselectivity by substrate modifications. The computed enantiomeric excess is found to be in reasonable agreement with the reported experimental stereoselectivities. A detailed investigation on the geometries of the crucial transition states reveals that apart from steric interactions between the α -substituent and MVK, various other factors such as orbital interactions and weak stabilizing hydrogen-bonding interactions play a vital role in stereoselectivity. The results serve to establish the importance of cumulative effects of various stabilizing and destabilizing interactions at the transition state as responsible for the stereochemical outcome of the reaction. The limitations of commonly employed qualitative propositions, relying on the steric protection of one of the prochiral faces of enamines offered by the bulky α -substituent, are presented.

Introduction

The area of organocatalysis has witnessed unprecedented growth in the recent times, and by now it is well recognized as an asymmetric protocol toward generating chiral compounds.¹

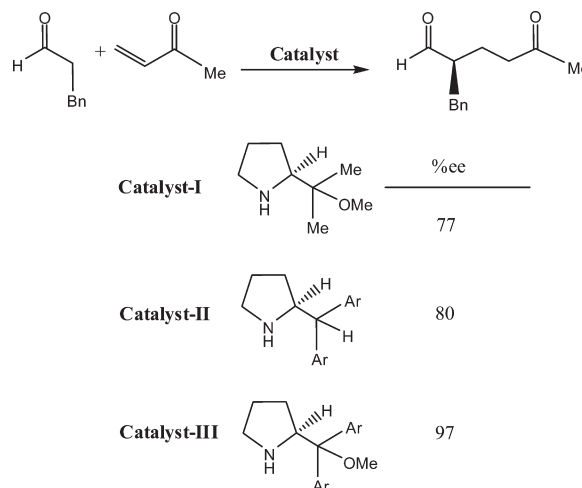
A large number of small organic molecules have been successfully employed as organocatalysts in enantioselective

(1) Bertelsen, S.; Jørgensen, K. A. *Chem. Soc. Rev.* **2009**, 38, 2178.

transformations.² Among these, chiral amines comprise one of the most versatile and useful class of organocatalysts.^{3,4} The primary motivation for employing secondary amines as a catalyst by far has been to activate carbonyl compounds through the generation of enamine or iminium ion intermediates in the catalytic cycle.⁴ The enamine/iminium catalysis using pyrrolidines consisting of bulky C α substituents has been proven to be effective in a diverse range of reactions from simple C–C bond formations to multistep cascade reactions.⁵

The general approach in catalyst design has been to provide the vital differential steric environments to the approaching electrophile or nucleophile. In other words, a sterically guided pathway through the pro-chiral faces holds the key to imparting successful stereoselectivity.⁶ While steric control is a major contributing factor, other weak interactions are also identified as critical to stereoselectivity.⁷ In fact, in a number of reactions, substrate activation has been proposed to involve hydrogen bonding interactions offered by an organocatalyst.⁸ The importance of weak interactions in stereoselective reactions catalyzed by proline and its analogues has earlier been established with the help of computational studies.⁹ A closer examination of these reports reveals that the focus has been predominantly on proline and its analogues. The most popular organocatalysts, including the prototypical L-proline, revolves around modifications of either the carboxylic group or elaborations at the β and γ positions of the pyrrolidine ring.¹⁰ It is worth

SCHEME 1. Michael Addition of Aldehyde to Enone Catalyzed by Chiral Pyrrolidines^{13a}



reckoning that in an ample number of instances, catalysts such as diphenylprolinol silyl ether have been found to be more effective among the proline analogues toward achieving high levels of stereoselectivity.¹¹ However, attempts to provide a molecular-level understanding of the factors that help impart high stereoselectivity with such popular catalysts are rather limited. The cumulative role of weak interactions and steric factors in the case of α -substituted pyrrolidine have not been systematically studied as yet.^{6,7}

Recently, Jørgensen and co-workers have demonstrated the first direct enantioselective Michael addition of simple aldehydes to enones by using α -substituted pyrrolidines as catalysts.¹² Improvements on the rate as well as stereoselectivities in such Michael additions are subsequently reported by Gellman et al. with the help of suitable cocatalysts.¹³ The reaction further exhibits interesting variations in enantioselectivities depending on the nature of the pyrrolidine α -substituent as summarized in Scheme 1.

Although a range of catalysts have been attempted for asymmetric Michael additions, a very few of them are found to be effective in imparting high enantioselectivity.^{12,13} It is also of timely relevance to note that similar catalysts and reactions are now increasingly employed in organocatalytic cascade reactions toward the synthesis of complex target molecules.¹⁴ Hence, a detailed analysis of the key transition states responsible for stereoselectivity induced by α -substituted pyrrolidines is highly desirable. Insights thus obtained could be useful in the rational design of new organocatalysts for asymmetric reactions. As a continuation of our endeavors in obtaining mechanistic insights on organocatalytic reactions,¹⁵ we have undertaken a comprehensive investigation toward unraveling the stereoselectivity-controlling factors in enantioselective Michael reaction between aldehydes

(2) (a) Dalko, P. I.; Moison, I. *Angew. Chem., Int. Ed.* **2001**, *40*, 3726. (b) List, B. *Tetrahedron* **2002**, *58*, 5573. (c) Dalko, P. I.; Moison, I. *Angew. Chem., Int. Ed.* **2004**, *43*, 5138. (d) Seayad, J.; List, B. *Org. Biomol. Chem.* **2005**, *3*, 719. (e) Gaunt, M. J.; Johansson, C. C. C.; McNally, A.; Vo, N. T. *Drug Discovery Today* **2007**, *12*, 8. (f) Pellissier, H. *Tetrahedron* **2007**, *63*, 9267.

(3) (a) Tsoogoeva, S. B. *Eur. J. Org. Chem.* **2007**, 1701. (b) List, B. *Chem. Commun.* **2006**, 819. (c) Mukherjee, S.; Yang, J. W.; Hoffmann, S.; List, B. *Chem. Rev.* **2007**, *107*, 5471 and references therein.

(5) (a) Marigo, M.; Schulte, T.; Franzen, J.; Jørgensen, K. A. *J. Am. Chem. Soc.* **2005**, *127*, 15710. (b) Marigo, M.; Bertelsen, S.; Landa, A.; Jørgensen, K. A. *J. Am. Chem. Soc.* **2006**, *128*, 5475. (c) Brandau, S.; Maerten, E.; Jørgensen, K. A. *J. Am. Chem. Soc.* **2006**, *128*, 14986. (d) Enders, D.; Huttli, M. R. M.; Grondal, C.; Raabe, G. *Nature* **2006**, *441*, 861. (e) Carlone, A.; Cabrera, S.; Marigo, M.; Jørgensen, K. A. *Angew. Chem., Int. Ed.* **2007**, *46*, 1101.

(6) Dinér, P.; Kjærsgaard, A.; Lie, M. A.; Jørgensen, K. A. *Chem.—Eur. J.* **2008**, *14*, 122.

(7) (a) Shinisha, C. B.; Sunoj, R. B. *Org. Biomol. Chem.* **2008**, *6*, 3921. (b) Marcelli, T.; Hammer, P.; Himo, F. *Chem.—Eur. J.* **2008**, *14*, 8562. (c) Bassan, A.; Zou, W.; Reyes, E.; Himo, F.; Cordova, A. *Angew. Chem., Int. Ed.* **2005**, *44*, 7028.

(8) (a) Schreiner, P. R. *Chem. Soc. Rev.* **2003**, *32*, 289. (b) Pihko, P. M. *Angew. Chem., Int. Ed.* **2004**, *43*, 2062. (c) Dessole, G.; Herrera, R. P.; Ricci, A. *Synlett* **2004**, 2374. (d) Marcelli, T.; Van Der Hass, R. N. S.; Van Maarseveen, J. H.; Hiemstra, H. *Angew. Chem., Int. Ed.* **2006**, *45*, 929. (e) McGilvra, J. D.; Unni, A. K.; Modi, K.; Rawal, V. H. *Angew. Chem., Int. Ed.* **2006**, *45*, 6130.

(9) (a) Clemente, F. R.; Houk, K. N. *Angew. Chem., Int. Ed.* **2004**, *43*, 5766. (b) Cheong, P. H.-Y.; Houk, K. N. *J. Am. Chem. Soc.* **2004**, *126*, 13912. (c) Clemente, F. R.; Houk, K. N. *J. Am. Chem. Soc.* **2005**, *127*, 11294. (d) Gordillo, R.; Houk, K. N. *J. Am. Chem. Soc.* **2006**, *128*, 3543. (e) Shinisha, C. B.; Sunoj, R. B. *Org. Biomol. Chem.* **2007**, *5*, 1287.

(10) (a) Cobb, J. A.; Shaw, D. M.; Longbottom, D. A.; Gold, J. B.; Ley, S. V. *Org. Biomol. Chem.* **2005**, *3*, 84. (b) Hayashi, Y.; Sumiya, T.; Takahashi, J.; Gotoh, H.; Urushima, T.; Shoji, M. *Angew. Chem., Int. Ed.* **2006**, *45*, 958. (c) Zu, L.; Wang, J.; Li, H.; Wang, W. *Org. Lett.* **2006**, *8*, 3007. (d) Luo, S.; Mi, L.; Zhang, L.; Liu, S.; Xu, H.; Cheng, J.-P. *Angew. Chem., Int. Ed.* **2006**, *45*, 3093.

(11) (a) Hayashi, Y.; Gotoh, H.; Hayashi, T.; Shoji, M. *Angew. Chem., Int. Ed.* **2005**, *44*, 4212. (b) Hayashi, Y.; Itoh, T.; Aratake, S.; Ishikawa, H. *Angew. Chem., Int. Ed.* **2008**, *47*, 2082. (c) Hayashi, Y.; Itoh, T.; Ohkubo, M.; Ishikawa, H. *Angew. Chem., Int. Ed.* **2008**, *47*, 4722. (d) Hayashi, Y.; Aratake, S.; Imai, Y.; Hibino, K.; Chen, Q. Y.; Yamaguchi, J.; Uchimaru, T. *Chem. Asian J.* **2008**, *3*, 225.

(12) Melchiorre, P.; Jørgensen, K. A. *J. Org. Chem.* **2003**, *68*, 4151.

(13) (a) Chi, Y.; Gellman, S. M. *Org. Lett.* **2005**, *7*, 4253. (b) Peelen, T. J.; Chi, Y.; Gellman, S. M. *J. Am. Chem. Soc.* **2005**, *127*, 11598.

(14) (a) Cabrera, S.; Alemán, J.; Bolze, P.; Bertelsen, S.; Jørgensen, K. A. *Angew. Chem., Int. Ed.* **2008**, *47*, 121. (b) Wang, Y.; Han, R.-G.; Zhao, Y.-L.; Yang, S.; Xu, P.-F.; Dixon, D. J. *Angew. Chem., Int. Ed.* **2009**, *48*, 9834. (c) McGarraugh, P. G.; Brenner, S. E. *Org. Lett.* **2009**, *11*, 5654. (d) Liu, Y.-K.; Ma, C.; Jiang, K.; Liu, T.-Y.; Chen, Y.-C. *Org. Lett.* **2009**, *11*, 2848. (e) Ruano, J. L. G.; Marcos, V.; Suanzes, J. A.; Marzo, L.; Alemán, J. *Chem.—Eur. J.* **2009**, *15*, 6576.

and enones catalyzed by three pyrrolidine variants. The results obtained using a model system as well as real systems for the Michael addition reactions are summarized in the following sections.

Computational Methods

All stationary points such as reactants, intermediates, and transition states were fully optimized in the gas phase at the mPW1PW91/6-31G* as well as the B3LYP/6-31G* levels of theory¹⁶ using Gaussian03 suite of quantum chemical programs.¹⁷ Though the use of B3LYP has recently been questioned for its ability to represent hydrogen bonding interactions,¹⁸ problems as discussed here, wherein the relative energies are of prime importance, continue remain successful with the B3LYP functional. In the present paper, we have used two functionals, namely, the mPW1PW91 and the B3LYP. The choice of modified Perdew–Wang functional is based on the available reports that the mPW1PW91 is good in accounting for the likely long-range interactions as well as hydrogen bonding.¹⁹ For select examples, we have also compared our results obtained by using these functionals with higher order composite ab initio methods such as the CBS-4M.^{20,21}

The stationary points thus obtained were subsequently subjected to single-point energy calculations at the PCM_(THF)/mPW1PW91/6-311G** and PCM_(THF)/B3LYP/6-311G** levels of theories by using Tomasi's polarized continuum model (PCM) with the United-Atoms Kohn–Sham (UAKS) radii.²² In the condensed phase, the $G_{\text{solvation}}$ obtained by using the PCM method comprises the electronic energy of the polarized solute and electrostatic solute–solvent interaction. Further, the ZPVE, thermal, and entropic corrections obtained at 298.5 K and 1 atm pressure from the gas-phase calculations have been

applied to the “bottom-of-the-well” energies obtained from the single-point energy evaluations in the condensed phase. Hence, the Gibbs free energies referred to in the text includes the entropic contributions estimated in the gas phase by using the standard harmonic oscillator and rigid rotor approximations. Similar methods have been employed earlier in related studies.²³ The inclusion of diffuse functions in the basis set are avoided for the PCM single-point energy calculations as this could lead to electron density tails permeate beyond the solute cavities generated by the molecularly shaped interlocking spheres. It has also been reported that the use of more extended basis sets often worsen the results obtained using continuum models.²⁴ However, to examine the basis set effects on the trends in the computed activation barriers, single-point energies were also evaluated at the mPW1PW91 level of theory by using 6-311+G** basis set. These results are tabulated in Table S2 in Supporting Information.

The optimized geometries were characterized as stationary points on the potential energy surface at respective levels of theories by evaluating the vibrational frequencies. The transition states were characterized by one and only one imaginary frequency. These frequencies were identified as representing the correct reaction coordinate, first by visual inspection of the imaginary frequency. The intrinsic reaction coordinate (IRC) calculations were subsequently carried out at the mPW1PW91/6-31G* level of theory to further authenticate the transition states.²⁵ The minimum energy IRC trajectories are plotted for all the transition states. These plots are provided in Supporting Information (Figures S9–S15). Further, we have carried out 10% displacement of the transition state geometry along the direction of the imaginary vibrational frequency and subsequently reoptimized the perturbed structure using the ‘calcfc’ option available in the program. This was to ensure whether the transition state is genuine and connects to the desired reactants and product.

The wave functions obtained through the above-mentioned methods were analyzed further to obtain certain electronic properties of the transition states. Weinhold's Natural Bond Orbital analysis has been performed by using NBO 3.1 program to compute the natural charges.²⁶ Topological analysis of the electron densities within Bader's Atoms-in-Molecule²⁷ (AIM) framework was carried out by using AIM2000 software.²⁸ Both NBO and AIM analyses were performed at the mPW1PW91/6-311G**/mPW1PW91/6-31G* level of theory. These data on important stationary points are employed to support some of the key points discussed in the text. The details of NBO and AIM analysis are provided in Supporting Information (Figure S2 and Figures S6–S8). Further, dispersion corrections (van der Waal effects) are calculated at the B3LYP-D level by using XYZ viewer program to get a qualitative estimate of the van der

(15) (a) Patil, M. P.; Sunoj, R. B. *J. Org. Chem.* **2007**, *72*, 8202. (b) Patil, M. P.; Sunoj, R. B. *Chem.—Eur. J.* **2008**, *14*, 10472. (c) Janardanan, D.; Sunoj, R. B. *J. Org. Chem.* **2008**, *73*, 8163. (d) Roy, D.; Patel, C.; Sunoj, R. B. *J. Org. Chem.* **2009**, *74*, 6936. (e) Shinisha, C. B.; Sunoj, R. B. *Org. Lett.* **2009**, *11*, 3242. (f) Sharma, A. K.; Sunoj, R. B. *Angew. Chem., Int. Ed.* **2010**, *49*, 6373.

(16) (a) Perdew, J. P.; Chevary, S. H.; Vosko, K. A.; Jackson, K. A.; Pederson, M. R.; Singh, D. J.; Fiolhais, C. *Phys. Rev. B* **1992**, *46*, 6671. (b) Perdew, J. P.; Chevary, S. H.; Vosko, K. A.; Jackson, K. A.; Pederson, M. R.; Singh, D. J.; Fiolhais, C. *Phys. Rev. B* **1993**, *48*, 4978. (c) Perdew, J. P.; Burke, K.; Wang, Y. *Phys. Rev. B* **1996**, *54*, 16533. (d) Adamo, C.; Barone, V. *J. Chem. Phys.* **1998**, *108*, 664. (e) Becke, A. D. *J. Chem. Phys.* **1993**, *98*, 5648. (f) Lee, C.; Yang, W.; Parr, R. G. *Phys. Rev. B* **1988**, *37*, 785.

(17) Frisch, M. J. et al. *Gaussian 03 Revision C.02*; Gaussian, Inc.: Wallingford, CT, 2004. See Supporting Information for full citation.

(18) (a) Woodcock, H. L.; Schaefer, H. F., III; Schreiner, P. R. *J. Phys. Chem. A* **2002**, *106*, 11923. (b) Schreiner, P. R.; Fokin, A. A.; Pascal, R. A., Jr.; de Meijere, A. *Org. Lett.* **2006**, *8*, 3635. (c) Zhao, J.; Truhler, D. G. *J. Chem. Theory Comput.* **2007**, *3*, 289. (d) Wodrich, M. D.; Corminboeuf, C.; Schreiner, P. R.; Fokin, A. A.; Schleyer, P. v. R. *Org. Lett.* **2007**, *9*, 1851. (e) Grimme, S.; Steinmetz, M.; Korth, M. *J. Chem. Theory Comput.* **2007**, *3*, 42.

(19) Some select examples of the successful application of the mPW1PW91 functional: (a) Pelek, A.; Carr, R. W. *J. Phys. Chem. A* **2001**, *105*, 4697. (b) Porembski, M.; Weisshaar, J. C. *J. Phys. Chem. A* **2001**, *105*, 6655. (c) Klein, R. A.; Mennucci, B.; Tomasi, J. *J. Phys. Chem. A* **2004**, *108*, 5851. (d) Klein, R. A.; Zottala, M. A. *Chem. Phys. Lett.* **2006**, *419*, 254. (e) Zhao, Y.; Truhlar, D. G. *J. Phys. Chem. A* **2004**, *108*, 6908. (f) Pinto, S. S.; Diogo, H. P.; Guedes, R. C.; Cabral, B. J. C.; da Piedade, M. E. M.; Simoes, A. M. *J. Phys. Chem. A* **2005**, *109*, 9700.

(20) (a) Ochterski, J. W.; Peterson, G. A.; Montgomery, J. A., Jr. *J. Chem. Phys.* **1996**, *104*, 2598. (b) Montgomery, J. A., Jr.; Frisch, M. J.; Ochterski, J. W.; Peterson, G. A. *J. Chem. Phys.* **2000**, *112*, 6532.

(21) The CBS-4M is known to give highly accurate energies for organic reactions/systems. Some select examples: (a) Roy, D.; Sunoj, R. B. *Org. Lett.* **2007**, *9*, 4873. (b) Antonello, S.; Benassi, R.; Gavioli, G.; Taddei, F.; Maran, F. *J. Am. Chem. Soc.* **2002**, *124*, 7529. (c) O'Hair, R. A. J.; Androutsopoulos, N. K. *Org. Lett.* **2000**, *2*, 2567.

(22) (a) Cossi, M.; Barone, V.; Cammi, R.; Tomasi, J. *Chem. Phys. Lett.* **1996**, *255*, 327. (b) Cancès, E.; Mennucci, B.; Tomasi, J. *J. Chem. Phys.* **1997**, *107*, 3032. (c) Cossi, M.; Scalmani, G.; Rega, N.; Barone, V. *J. Chem. Phys.* **2002**, *117*, 43.

(23) (a) Galano, A.; Francisco-Marquez, M. *J. Phys. Chem. B* **2009**, *113*, 11338. (b) Mora-Diez, N.; Keller, S.; Alvarez-Idaboy, J. R. *Org. Biomol. Chem.* **2009**, *7*, 3682. (c) Ardura, D.; López, R.; Sordo, T. L. *J. Phys. Chem. B* **2005**, *109*, 23618. (d) Carlqvist, P.; Eklund, R.; Brinck, T. *J. Org. Chem.* **2001**, *66*, 1193.

(24) (a) Foresman, J. B.; Keith, T. A.; Wiberg, K. B.; Snoonian, J.; Frisch, M. J. *J. Phys. Chem.* **1996**, *100*, 16098. (b) Takano, Y.; Houk, K. N. *J. Chem. Theory Comput.* **2005**, *1*, 70. (c) Sadlej-Sosnowska, N. *Theor. Chem. Acc.* **2007**, *118*, 281.

(25) (a) Gonzalez, C.; Schlegel, H. B. *J. Chem. Phys.* **1989**, *90*, 2154. (b) Gonzalez, C.; Schlegel, H. B. *J. Phys. Chem.* **1990**, *94*, 5523.

(26) (a) Glendening, E. D.; Reed, A. E.; Carpenter, J. E.; Weinhold, F. *NBO Version 3.1*; Gaussian, Inc.: Wallingford, CT, 2009. (b) Reed, A. E.; Curtiss, L. A.; Weinhold, F. *Chem. Rev.* **1988**, *88*, 899.

(27) Bader, R. F. W. *Atoms in Molecules: A Quantum Theory*; Clarendon Press: Oxford, 1990.

(28) (a) *AIM2000 Version 2.0*; Büro für Innovative Software, SBK-Software: Bielefeld, Germany, 2002. (b) Biegler-König, F.; Schonbohm, J.; Bayles, D. *J. Comput. Chem.* **2001**, *22*, 545. (c) Biegler-König, F.; Schonbohm, J. *J. Comput. Chem.* **2002**, *23*, 1489.

Waals effects. The calculated free energies of activation by inclusion of van der Waal effects are provided in Supporting Information (Table S4).²⁹

Results and Discussion

We have investigated an organocatalyzed Michael addition reaction between aldehydes and methyl vinyl ketone (MVK) to elucidate the origin and the role of pyrrolidine α -substituents in imparting high levels of stereoselectivity. Commonly employed catalysts with different α -substituents, as shown in Scheme 1, are chosen for this study. According to the most widely accepted mechanism, the secondary amine (pyrrolidine) promotes the addition of aldehyde to a Michael acceptor through iminium/enamine catalysis.³⁰ The nature of the catalyst, electronic and steric factors along with the cumulative effect of several weak interactions operating in the competing diastereomeric transition states, all would contribute to the stereochemical outcome. A comprehensive analysis is therefore undertaken first, wherein geometrically different modes of addition between a model enamine (derived from dimethylamine and propanal) and MVK are studied.³¹ In the subsequent section, discussions on the stereoselectivity for the real-life catalytic systems are provided.

Stereochemical Descriptors. The enamine derived from dimethylamine and propanal is designated using *E* or *Z* configurational descriptors, depending on the relative orientations of the methyl and dimethylamino groups around the enamine double bond. The letters *c* and *t* are used to denote *s-cis*-MVK and *s-trans*-MVK. In the case of pyrrolidine enamines, *syn* and *anti* notations depict the orientation of the enamine double bond with respect to the α -substituent. The addition from the *si* and *re*-faces are indicated by *a-si*, *a-re*, *s-si* and *s-re*, where *a* and *s* stands for *anti*- and *syn*-enamine, respectively.

Model System. The model enamine derived from dimethylamine and propanal can have two isomers arising from *E/Z* configuration around the enamine double bond, whereas for MVK *s-cis* and *s-trans* conformers are possible. Different transition states (TSs) for the C–C bond formation arising as a result of the enamine configurations as well as conformers of MVK are examined. The knowledge of these different modes of addition is important to be able to identify the most favored approach between the enamine and electrophile. All key TSs are located at the mPW1PW91/6-31G* level of theory. The computed activation barriers for different addition modes are provided in Table 1. Among these

TABLE 1. Computed Gibbs Free Energy of Activation^a (in kcal/mol) for the Michael Addition of Enamine Derived from Dimethylamine and Propanal with Methyl Vinyl Ketone

method ^c	(<i>E</i>)- <i>c</i> 1	(<i>E</i>)- <i>c</i> 2	(<i>E</i>)- <i>c</i> 3
$\Delta G^\ddagger_{(\text{gas-phase})}$			
M1	26.0 (0.0)	26.2 (0.2)	28.4 (2.4)
M2	30.4 (0.2)	30.2 (0.0)	34.7 ^b (4.5)
M3	26.8 (0.0)	28.8 (2.0)	30.2 (3.4)
$\Delta G^\ddagger_{(\text{condensed-phase})}$			
M4	24.9 (0.0)	26.0 (1.1)	26.1 (1.2)
M5	29.0 (0.0)	29.7 (0.7)	31.2 ^b (2.2)

^aBarriers are computed with respect to the separated (*E*)-enamine and *cis*-MVK. ^bThe B3LYP/6-31+G* geometry is used. ^cM1: mPW1PW91/6-311G**//mPW1PW91/6-31G*. M2: B3LYP/6-311G**//B3LYP/6-31G*. M3: CBS-4M. M4: PCM_(THF)/mPW1PW91/6-311G**//mPW1PW91/6-31G*. M5: PCM_(THF)/B3LYP/6-311G**//B3LYP/6-31G*.

possibilities, three modes of addition involving (*E*)-enamine and *cis*-MVK, designated as (*E*)-*c*1, (*E*)-*c*2, and (*E*)-*c*3 in Figure 1, are identified to exhibit lower activation barriers,³² where the notations *c*1, *c*2, and *c*3 refer to different dihedral angle possibilities, around the incipient bond. The corresponding TSs for the (*Z*)-enamine are in general found to be higher in energy. It is noticed that (*E*)-*c*1 mode for the addition of (*E*)-enamine to *cis*-MVK is the most preferred mode.

In an effort to examine how the trends hold at higher levels of theory, the TSs for the addition of model-enamine to MVK are identified at the CBS-4 M level. It has been found that trends in the activation barriers for different modes of addition continue to remain the same even at higher level composite ab initio calculations. Further, with a select set of examples, the calculated barriers involving *trans*-MVK are found to be much higher as well.³² The present discussions are therefore confined to three lower barrier addition modes between (*E*)-enamine (*E*) and *cis*-MVK (*c*). Since the TSs are relatively more polar owing to the charge separation, we have also examined the role of implicit solvents by using a continuum dielectric model. While slightly different relative energies for TSs is noticed in the solvent phase, the most favored mode of addition remained the same ((*E*)-*c*1) as that noticed in the gas phase.

The optimized geometries of three lower energy TSs for the C–C bond formation are provided in Figure 1. The incipient bond C₃–C₄ in the TSs is found to be in the range of 1.8–2.0 Å, similar to that typically found in organocatalyzed C–C bond-forming reactions.³³ These TSs differ in terms of (i) the orientation of the C–C double bonds of the enamine moiety and MVK and (ii) the relative proximity between the carbonyl oxygen and the enamine nitrogen. In general, the double bonds are found to be *gauche* to each other. Further, with the help of AIM analyses three stabilizing intramolecular interactions and the corresponding bond critical points (*bcps*) are identified. These *bcps* in (*E*)-*c*1 mode are located along the bond path connecting atoms O₇···C₂, O₇···H (–Me group), and N₁···C₅ besides the one along the reaction coordinate (C₃–C₄).³⁴

(29) (a) Grimme, S. *J. Comput. Chem.* **2006**, *27*, 1787. (b) XYZ viewer Program available at <http://www.physto.se/~sven/>. Accessed on September 17, 2010.

(30) For a detailed comparison between the energetic preferences associated with the generation of iminium and enamine intermediates, see: Patil, M. P.; Sunoj, R. B. *Chem. Asian J.* **2009**, *4*, 714.

(31) Reports on nonstereoselective versions of the Michael addition of aldehyde to enone in the presence of achiral amine are also available. See: (a) Hagiwara, H.; Okabe, T.; Hakoda, K.; Hoshi, T.; Ono, H.; Kamat, V. P.; Suzuki, T.; Ando, M. *Tetrahedron Lett.* **2001**, *42*, 2705. (b) Shimizu, K.; Suzuki, H.; Hayashi, E.; Kodama, T.; Tsuchiya, Y.; Hagiwara, H.; Kitayama, Y. *Chem. Commun.* **2002**, 1068. (c) Hagiwara, H.; Komatsubara, N.; Ono, H.; Okabe, T.; Hoshi, T.; Suzuki, T.; Ando, M.; Kato, M. *J. Chem. Soc., Perkin Trans. 1* **2001**, 316.

(32) The TSs for the addition step for different isomers of enamine (*E/Z*) as well as MVK (*cis/trans*) are also located at the mPW1PW91/6-31G*, B3LYP/6-31G*, and CBS-4 M levels of theories. A summary of the activation barriers obtained at these levels of theories for all TSs is provided in Table S1 in Supporting Information.

(33) (a) Allemann, C.; Gordillo, R.; Clemente, F. R.; Cheong, P. H.-Y.; Houk, K. N. *Acc. Chem. Res.* **2004**, *37*, 570. (b) Zhao, J.-Q.; Gan, L.-H. *Eur. J. Org. Chem.* **2009**, 2661.

(34) Details of AIM analysis for all other modes of addition are provided in Figure S1 in the Supporting Information.

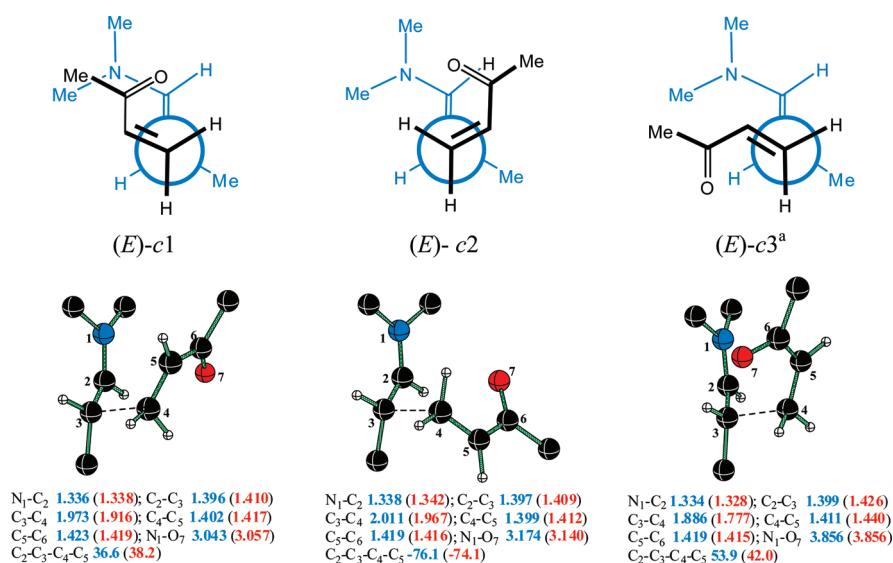


FIGURE 1. mPW1PW91/6-31G* optimized geometries for the addition of (*E*)-enamine (derived from dimethylamine and propanal) to *cis*-MVK. The values in parentheses refer to the optimized bond lengths and angles obtained at the B3LYP/6-31G* level of theory. Atom colors: black = C, red = O, blue = N. Angles are given in degrees and distances in Å.

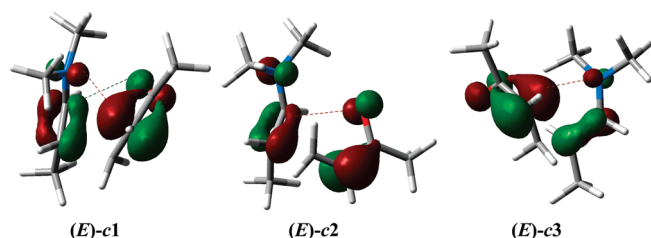


FIGURE 2. Frontier Kohn-Sham orbital contours generated at the mPW1PW91/6-311G**/mPW1PW91/6-31G* level of theory for transition states for (*E*)-c1, (*E*)-c2, and (*E*)-c3 modes of addition. (See Figure 1 for the atom numbering scheme as used in the text.)

To identify the factors that influence the predicted relative energy order between the above TSs, we have carefully analyzed Coulombic as well as orbital interactions. The charges on the enamine nitrogen and the oxygen of MVK are found to be negative.³⁵ The frontier Kohn-Sham orbitals of the TSs revealed interesting orbital interactions between the Michael donor and acceptor. Although the role of orbital interactions in organocatalyzed reactions is not commonly reported, the selectivity issues in several Diels-Alder reactions have been explained with the help of secondary orbital interaction (SOI) protocol.³⁶ The key Kohn-Sham frontier orbitals generated at the mPW1PW91/6-311G**/mPW1PW91/6-31G* level of theory for three modes of addition are provided in Figure 2. Two important types of orbital interactions are evident. These include the interaction between

the lone pair of (i) enamine nitrogen and the developing C₅-C₆ π -bond of MVK and (ii) the carbonyl oxygen and the enamine C₂-C₃ π -bond (see Figure 1 for atom numbering). The efficiency of these orbital interactions will evidently depend on the orientation of the carbonyl group and the developing C₅-C₆ double bond of MVK with respect to the enamine nitrogen. For instance, orbital interaction of the type-i is not possible in the case of (*E*)-c2 mode of addition, as the C₅-C₆ bond of MVK is oriented away from the enamine nitrogen. On the other hand, the type-ii orbital interaction can contribute toward the stabilization of (*E*)-c1 and (*E*)-c2 modes. In (*E*)-c3 mode, the carbonyl oxygen is oriented away and results in lack of interaction with the enamine C₂-C₃ π -bond. The additional orbital interactions in (*E*)-c1 TS as compared to that in (*E*)-c2 and (*E*)-c3 could be regarded as the key reason for (*E*)-c1 being the most favored mode of addition. The above analyses thus convey the origin of the likely geometric preferences for the addition between enamine and MVK. It can further be envisaged that the enamines derived from pyrrolidines bearing bulky α -substituents could exhibit a preference for the (*E*)-c1 mode of addition. This observation is particularly relevant in light of the limited rotameric possibilities around the newly developing C-C bond owing to the presence of larger α -substituents on the pyrrolidine ring.

Another interesting observation that emerged during this investigation relates to the possibility of side products. The characteristic imaginary frequency of the TS for the addition step is found to be predominantly C₃-C₄ bond vibration coupled with a relatively minor displacement along the O₇-C₂ bond. More significantly, *walking down* by following the transition vector toward the product side by using the intrinsic reaction coordinate (IRC) calculations resulted in the formation of a cyclic pyran intermediate. It is of significance to note that Michael additions are also known to often proceed through a hetero-Diels-Alder pathway, first to form a cyclic intermediate, which upon subsequent hydrolysis furnishes the desired Michael product.³⁷

(35) The charges obtained by using the natural population analysis at the mPW1PW91/6-311G**/mPW1PW91/6-31G* level of theory on the TS revealed negative charges on oxygen (-0.7) of the developing alkoxide as well as on the nitrogen (-0.4) of the enamine moiety. See Figure S2 in Supporting Information.

(36) (a) Birney, D. M.; Houk, K. N. *J. Am. Chem. Soc.* **1990**, *112*, 4127. (b) Singleton, D. A. *J. Am. Chem. Soc.* **1992**, *114*, 6563. (c) Ohwada, T. *Chem. Rev.* **1999**, *99*, 1337. (d) Arrieta, A.; Cossio, F. A. *J. Org. Chem.* **2001**, *66*, 6178. (e) Arrieta, A.; Cossio, F. P.; Lecea, B. *J. Org. Chem.* **2001**, *66*, 6178. (f) Patil, M. P.; Sunoj, R. B. *Org. Biomol. Chem.* **2006**, *4*, 3923. (g) Wannere, C. S.; Paul, A.; Herges, R.; Houk, K. N.; Schaefer, H. F., III; Schleyer, P. v. R. *J. Comput. Chem.* **2007**, *28*, 344.

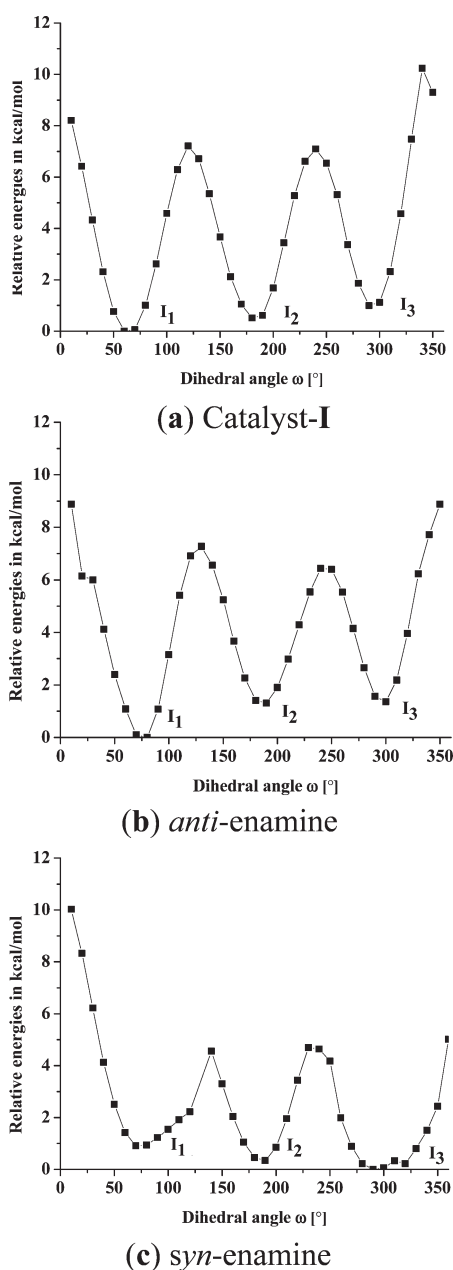
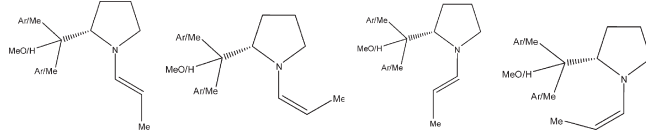


FIGURE 3. Relaxed potential energy scans generated at the mPW1PW91/6-31G* level of theory with respect to ω (N-C α -C-X, where X = -OMe) for (a) catalyst **I** and the corresponding (b) *anti*-enamine and (c) *syn*-enamine, derived from catalyst **I** and propanal.

Real Systems. α -Pyrrolidine Catalysts. After having identified the important modes of addition between the model enamine and MVK, we turned our attention to pyrrolidine enamines. The major focus here is to obtain improved insights into the role of the most commonly employed pyrrolidine α -substituents toward imparting stereoselectivity in

(37) (a) For experimental reports on the formation of a six-membered cyclic product (pyran derivative in the case of addition of propanal to MVK) in Michael reaction, see Ref 13b and Seebach, D.; Brook, M. A. *Helv. Chim. Acta* **1985**, 68, 319. (b) Additional computations, starting from a perturbed geometry derived from the transition state by a 10% displacement along the reaction coordinates, confirms the formation of a pyran. See Figure S3 in Supporting Information.

TABLE 2. Relative Energies (in kcal/mol) between Different Configurations and Conformers of Enamines Derived from Catalysts **I**, **II**, or **III** and Propanal Computed at the mPW1PW91/6-311G**//mPW1PW91/6-31G* Level of Theory^a

catalyst	ω^b				
		(E)-a	(Z)-a	(E)-s	(Z)-s
I ₁	60	0.0 (0.0)	2.8 (2.9)	3.1 (3.3)	7.9 (8.1)
I ₂	180	1.4 (1.7)	2.9 (3.2)	2.1 (2.3)	7.0 (7.4)
I ₃	300	1.4 (1.6)	3.2 (3.6)	1.8 (2.3)	6.8 (7.3)
II ₁	60	0.0 (0.0)	3.8 (3.9)	1.7 (1.6)	6.0 (6.0)
II ₂	180	1.0 (0.8)	5.1 (4.8)	3.6 (3.5)	9.2 (9.0)
II ₃	300	0.1 (−0.2)	4.1 (3.8)	2.3 (2.2)	7.2 (6.8)
III ₁	60	0.0 (0.0)	4.2 (4.2)	3.0 (3.1)	7.8 (7.8)
III ₂	180	6.1 (6.2)	9.4 (9.5)	3.7 (3.8)	8.7 (8.9)
III ₃	300	1.6 (1.8)	5.2 (5.4)	4.8 (5.0)	13.2 (13.4)

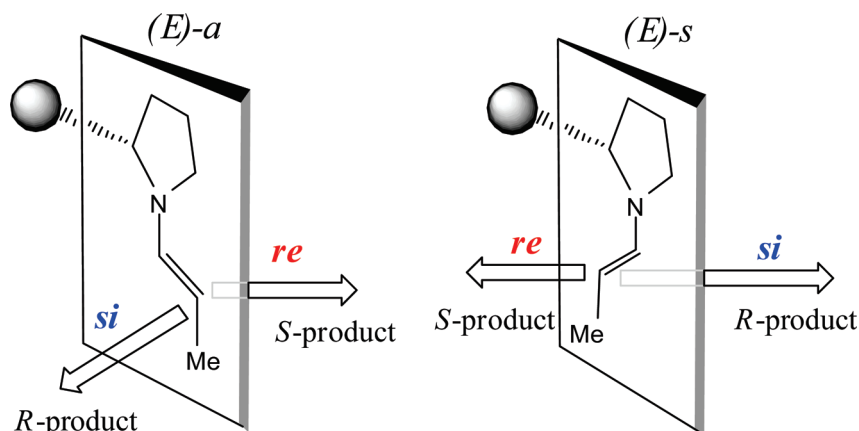
^aThe values in parentheses indicate energies obtained at the PCM_(THF)/mPW1PW91/6-311G**//mPW1PW91/6-31G* level of theory.
^b ω = N-C α -C-H/OMe

organocatalytic reactions. Three different α -substituents, namely, methoxydimethylmethyl, diphenylmethyl, and methoxydiphenylmethyl, are examined here (Scheme 1). It is important to note that several conformational possibilities for α -substituents are likely. A detailed conformational analysis of the α -substituents in these catalysts is therefore performed first. The potential energy scans with respect to the dihedral angle ω (N-C α -C-X, where X = -OMe), defining the orientation of the α -substituent, is carried out. A representative scan from 0 to 360° for the catalyst **I** is provided in Figure 3a.³⁸ The conformational space evidently presents three distinct minima with ω values around 60°, 180°, and 300°. These minimum energy geometries obtained through the PES scans are subjected to further geometry optimization and frequency calculations. All three conformers (**I**₁, **I**₂, and **I**₃) are found to be stationary points exhibiting all real frequencies within 1 kcal/mol energy difference between them.

Next, different conformers of the enamines derived from these catalysts and propanal are considered. In addition to (*E*)- and (*Z*)-configurations around the enamine double bond, conformers arising as a result of the *syn* (*s*) and *anti* (*a*) orientations of the enamine double bond, with respect to the pyrrolidine α -substituent, are also identified. The plot obtained through relaxed potential energy scans for *anti*- as well as *syn*-enamines are provided respectively in Figure 3b and c. Similar to the parent α -substituted pyrrolidines, three minima for both *anti*- and *syn*-enamines are identified in (*E*)- and (*Z*)-enamine configurations. The relative energies of 12 such enamine isomers are provided in Table 2. The results evidently exhibit a preference for the (*E*)-*a* isomer of enamine for all three pyrrolidines. The energy difference between the lowest and the other higher energy enamine isomers are larger with catalysts **II** and **III** as compared to that with catalyst **I**. Further, the (*Z*)-*s* isomer is found to be the highest energy enamine, a result of the inherent steric interaction

(38) The PES maps for other catalysts (catalyst **II** and catalyst **III**) as well as the corresponding *anti*- and *syn*-enamines (derived from these catalysts and propanal) are provided in Supporting Information. See Figures S4 and S5.

SCHEME 2. Illustration of different stereochemical modes of additions between pyrrolidine enamine of propanal (1) and MVK responsible for the formation of stereoisomeric products



between the methyl group and the pyrrolidine α -substituent. In general, the *syn* orientation of the enamine double bond is less favored owing to its proximity with the bulky group at the pyrrolidine α -position. The aforementioned conformational analyses enabled us to understand the differential steric environments around the nucleophilic carbon on different enamines. On the basis of the larger spread of enamine energies, the participation of (*Z*)-enamine in the C–C bond formation can be assumed to be less likely. The approach between (*Z*)-enamine and MVK is quite unlikely to be fruitful because of the apparent steric crowding.³⁹

Transition State Analysis. Two important enamine conformers, namely, (*E*)-*a* and (*E*)-*s*, are considered in greater detail in the stereoselectivity-controlling C–C bond-formation step. Four key modes of addition between *syn*- or *anti*- enamines and MVK through their prochiral faces (*re*/*si*) are depicted in Scheme 2. We have chosen two of the most commonly employed aldehydes in Michael addition reactions, namely, propanal (1) and 3-phenyl propanal (2), as the nucleophilic partner for the present investigation. The addition of (*E*)-*a* or (*E*)-*s* enamine derived from 1 to MVK through the *si* face will lead to *R*-product, whereas the *re* face addition will result in *S*-product. This trend will apparently appear to be opposite in the case of 3-phenyl propanal (2), due to the changes in the priority order of the groups attached to the asymmetric carbon.⁴⁰ Since the *si* face of (*E*)-*s* enamine is evidently blocked by the bulky pyrrolidine α -substituent, such higher-energy TSs are excluded from further analysis. Instead, more attention is paid to the lower energy TSs along the competing diastereomeric pathways.

Although the number of stereochemical modes of addition between enamine and MVK could be large, as described in the previous sections, only the lower-energy TSs that hold the key to the formation of enantiomeric products are

considered here in greater detail. The computed activation barriers, both in the gas phase and in the condensed phase, for the reaction of the enamines derived from (a) 1 or (b) 2 with MVK are respectively provided in Tables 3 and 4. The comparison of the relative energies of TSs for catalysts **I**, **II**, and **III** conveys that the (*E*)-*a*-*si* addition of enamine to MVK is the most favored mode in the condensed phase as revealed by the $\Delta G^\ddagger_{\text{THF}}$ values. The computed relative energies of the TSs in the case of propanal (1) suggest that the product selectivity is in favor of the *R* enantiomer for catalysts **I**, **II**, and **III** (Table 3).

In an earlier study, Gellman and co-workers have demonstrated that catalyst **III** is quite effective toward imparting high stereoselectivity in Michael addition reactions over a wide range of substrates whereas the performance of catalysts **I** and **II** is found to be only modest.^{13a} The enantiomeric excess predicted by using the relative energies of diastereomeric pair of TSs at the $\text{PCM}_{(\text{THF})}/\text{B3LYP}/6\text{-}311\text{G}^{**}$ level of theory (M4) for 3-phenyl propanal (2) exhibits good agreement with the experimentally reported values for all catalysts (Table 4).⁴¹ However, the $\text{PCM}_{(\text{THF})}/\text{mPW1PW91}/6\text{-}311\text{G}^{**}$ values are found to be not in very good accord in the case of catalyst **II**. In general, the inclusion of solvation effects through continuum model is found to be effective toward obtaining reasonably correct estimates on the stereochemical outcome of this reaction. It is worth noting at this juncture that the stereoselectivities in C–C bond-forming reactions computed on the basis of the relative energies of diastereomeric TSs obtained through DFT computations have been reported to be quite good.⁴² The single-point energy calculations in the condensed phase on the gas-phase geometries appear to be suitable for a correct description with the present series of examples.

(39) The TSs involving the attack of (*Z*)-enamine to electrophile are also located (see Table S1 in Supporting Information). However, the *E*-isomer of enamine is found to be more stable than the *Z*-form by about 3–4 kcal/mol at the $\text{mPW1PW91}/6\text{-}311\text{G}^{**}/\text{mPW1PW91}/6\text{-}31\text{G}^*$ level of theory, both in the gas phase as well as in the solvent phase. Moreover, the conversion of (*E*)-enamine to (*Z*)-enamine is found to have a very high barrier (~60 kcal/mol) at the same level of theory. Hence, only (*E*)-enamines are considered for further investigations.

(40) The addition of (*E*)-*a* or (*E*)-*s* pyrrolidine enamines derived from 3-phenyl propanal (2) to MVK, through the *si* face will lead to *S*-product, whereas the *re* face addition will result in *R*-product.

(41) It has also been reported that the use of cocatalyst such as catechol can improve the selectivity in some cases ref.^{13a} In order to examine the effect of cocatalyst on the predicted selectivity, all relevant TSs are remodeled using an explicit methanol molecule. Since the cocatalyst is expected to stabilize the developing alkoxide ion at the TSs, the explicit methanol molecule is placed around the oxygen atom of MVK. The activation parameters for the methanol-assisted pathways obtained at the $\text{mPW1PW91}/6\text{-}31\text{G}^*$ level of theory are provided in the Supporting Information, Table S3. The stereoselectivities computed for catalyst **III** at the $\text{PCM}_{\text{THF}}/\text{mPW1PW91}/6\text{-}311\text{G}^{**}/\text{mPW1PW91}/6\text{-}31\text{G}^*$ level of theory show reasonable agreement with the experimental values. Interestingly, in the case of catalysts **I** and **II** the enantioselectivity was found to be higher with the inclusion of explicit methanol as compared to the unassisted pathway.

TABLE 3. Computed Gibbs Free Energy of Activation^a (in kcal/mol) for the Michael Reaction between Pyrrolidine Enamines Derived from Propanal (**1**) and MVK along with the Corresponding Enantiomeric Excess

catalyst		(<i>E</i>)- <i>a</i> - <i>si</i> 1-TS-a	(<i>E</i>)- <i>a</i> - <i>re</i> 1-TS-b	(<i>E</i>)- <i>s</i> - <i>re</i> 1-TS-c	% ee predicted	% ee expt ^b
I	M1	26.6 (0.0)	28.4 (1.8)	27.0 (0.4)	<i>R</i> -(32)	<i>b</i>
	M2	25.6 (0.0)	26.2 (0.6)	26.4 (0.8)	<i>R</i> -(47)	
	M3	30.4 (0.0)	32.7 (2.3)	30.9 (0.5)	<i>R</i> -(40)	
	M4	28.9 (0.0)	30.0 (1.1)	30.0 (1.1)	<i>R</i> -(73)	
II	M1	25.7 (0.3)	25.4 (0.0)	27.9 (3.2)	<i>S</i> -(25)	<i>R</i> -(64) ^c
	M2	26.0 (0.0)	26.6 (0.6)	28.7 (2.6)	<i>R</i> -(47)	
	M3	29.7 (0.3)	29.4 (0.0)	31.5 (1.8)	<i>S</i> -(25)	
	M4	29.8 (0.0)	30.4 (0.6)	32.1 (2.3)	<i>R</i> -(47)	
III	M1	25.8 (0.0)	31.6 (5.8)	31.5 (5.7)	<i>R</i> -(99)	<i>b</i>
	M2	25.6 (0.0)	30.0 (4.4)	30.8 (5.2)	<i>R</i> -(99)	
	M3	29.9 (0.0)	35.6 (5.7)	35.3 (5.4)	<i>R</i> -(99)	
	M4	29.5 (0.0)	33.4 (4.0)	34.3 (4.9)	<i>R</i> -(99)	

^aM1: mPW1PW91/6-311G**//mPW1PW91/6-31G*. M2: PCM_(THF)/mPW1PW91/6-311G**//mPW1PW91/6-31G*. M3: B3LYP/6-311G**//B3LYP/6-31G*. M4: PCM_(THF)/B3LYP/6-311G**//B3LYP/6-31G*. The activation barriers are respect to *anti*-(*E*)-enamine and MVK. The values in parentheses are relative energies with respect to the lowest energy TS in each set. ^bExperimental values not available. ^cFor the addition of propanal to MVK catalyzed by (*S*)-2-[bis(3,5-dimethylphenyl)-methyl]pyrrolidine, which is quite similar to catalyst **II**.¹²

After having examined the energetic preferences for stereochemically distinct modes of addition, efforts were expended toward identifying the kind of stabilization/destabilization effects operating in these key TSs. In the next section, careful examination of TS geometries for each catalyst system is performed to gain insights into the factors that govern stereoselectivities, as predicted.

The optimized TS geometries for the addition of enamine of catalyst **I** derived from propanal (**1**) as well as 3-phenyl propanal (**2**) to *cis*-MVK are provided in Figure 4. The comparison of steric environments as well as other subtle factors is found to be useful indicators in rationalizing the relative energy order of the diastereomeric TSs. Three such key factors are identified, which include (i) stabilizing hydrogen bonding interactions, (ii) distortion of the enamine moiety, and (iii) the geometry of approach of MVK with respect to the pyrrolidine α -substituent. In the case of catalyst **I**, it is noticed that (*E*)-*a*-*si* and (*E*)-*s*-*re* modes of addition are relatively free from steric interactions between MVK and the α -substituent (more precisely, the methyl groups of the methoxydimethylmethyl group). Accordingly, the corresponding TSs, **1-TS-Ia** and **1-TS-Ic**, have comparable energies (Table 3). Similar feature is also noticed with 3-phenyl propanal, as revealed by the energies of **2-TS-Ia** and **2-TS-Ic** (Table 4). The presence of an improved hydrogen bonding interaction in **1-TS-Ic** (and **2-TS-Ic**) as compared to that in **1-TS-Ia** (and **2-TS-Ia**) is identified between the developing

TABLE 4. Computed Gibbs Free Energy of Activation^a (in kcal/mol) for the Michael Reaction between Pyrrolidine Enamines Derived from 3-Phenyl Propanal (**2**) with MVK along with the Corresponding Enantiomeric Excess

catalyst		(<i>E</i>)- <i>a</i> - <i>si</i> 2-TS-a	(<i>E</i>)- <i>a</i> - <i>re</i> 2-TS-b	(<i>E</i>)- <i>s</i> - <i>re</i> 2-TS-c	% ee predicted	% ee expt ^b
I	M1	27.1 (0.0)	29.0 (1.9)	27.7 (0.6)	<i>S</i> -(47)	77
	M2	26.5 (0.0)	27.7 (1.2)	27.5 (1.0)	<i>S</i> -(69)	
	M3	30.8 (0.0)	33.0 (2.2)	32.2 (1.4)	<i>S</i> -(83)	
	M4	29.8 (0.0)	31.2 (1.4)	31.6 (1.8)	<i>S</i> -(83)	
II	M1	26.8 (0.6)	26.2 (0.0)	30.8 (4.6)	<i>R</i> -(47)	80
	M2	27.4 (0.0)	27.9 (0.5)	30.9 (3.5)	<i>S</i> -(40)	
	M3	32.2 (2.3)	29.9 (0.0)	35.9 (6.0)	<i>R</i> -(96)	
	M4	32.7 (1.4)	31.3 (0.0)	35.5 (4.2)	<i>R</i> -(83)	
III	M1	25.8 (0.0)	33.9 (8.1)	33.3 (7.5)	<i>S</i> -(99)	97
	M2	25.7 (0.0)	33.0 (7.3)	32.6 (6.9)	<i>S</i> -(99)	
	M3	29.8 (0.0)	38.2 (8.4)	37.2 (7.4)	<i>S</i> -(99)	
	M4	29.4 (0.0)	36.9 (7.5)	36.2 (6.8)	<i>S</i> -(99)	

^aM1: mPW1PW91/6-311G**//mPW1PW91/6-31G*. M2: PCM_(THF)/mPW1PW91/6-311G**//mPW1PW91/6-31G*. M3: B3LYP/6-311G**//B3LYP/6-31G*. M4: PCM_(THF)/B3LYP/6-311G**//B3LYP/6-31G*. The activation barriers are respect to *anti*-(*E*)-enamine and MVK. The values in parentheses are relative energies with respect to the lowest energy TS in each set. ^bExperimental values are from ref 13a.

alkoxide oxygen and the pyrrolidine C α hydrogen. These hydrogen-bonding contacts have been further verified by using the electron density at the bond critical points within the AIM formalism.⁴³ Next, distortion of the enamine moiety in the TS is analyzed with the help of two pertinent dihedral angles. The first one is with respect to the pyrrolidine C α , i.e., θ_1 (C α -N₁-C₂-C₃) and θ_2 (C α' -N₁-C₂-C₃), and the second one is θ_3 (N₁-C₂-C₃-C_{3'}) as shown in Figure 4. The first two dihedral angles capture the changes associated with the orientation of the enamine double bond around N₁-C₂ bond and the effects of puckering of the pyrrolidine ring. The delocalization efficiency of the nitrogen lone pair (which in turn can be regarded as related to the nucleophilicity of enamine) could also be related to θ_1 and θ_2 . The third distortion parameter θ_3 essentially reflects the planarity of the C₂-C₃ double bond. The geometric distortion of the enamine moiety in the TS as compared to the parent enamine intermediate has been employed as a tool toward understanding the predicted relative energy order between diastereomeric TSs.^{7a,9c,9e}

The analysis of the above-mentioned distortion parameters has been carried out. The θ_1 , θ_2 , and θ_3 values for *anti*- and *syn*-enamine intermediates are compared with the corresponding values in the TSs. It is identified that the changes in θ_1 and θ_2 between the enamine and the corresponding values in the TSs do not present any general trends. However, θ_3 exhibits modest variations depending on the relative energy of the TSs. The largest deviations, as reflected in $\Delta\theta_3$, are noticed for **1-TS-Ib** and **2-TS-Ib**, whose energies are higher than other modes of addition (Figure 4). In general, the distortions are found to be nearly identical for both propanal and 3-phenyl propanal systems. These geometric features remain quite similar with other catalysts (**II** and **III**) as well.

The approach of electrophiles through the hindered face of the enamine is generally excluded from computational investigations, primarily on the qualitative premise that such a trajectory would experience high degree of steric interaction with the α -substituent. In the present study, we became curious to know how high the C-C bond formation barrier

(42) Some recent examples: (a) Domingo, L. R.; Pitcher, M. T.; Arroyo, P. *Eur. J. Org. Chem.* **2006**, 2570. (b) Gordillo, R.; Houk, K. N. *J. Am. Chem. Soc.* **2006**, 128, 3543. (c) Bertelsen, S.; Marigo, M.; Brandes, S.; Dinér, P.; Jørgensen, K. A. *J. Am. Chem. Soc.* **2006**, 128, 12973. (d) Fu, A.; List, B.; Thiel, W. *J. Org. Chem.* **2006**, 71, 320. (e) Yamanaka, M.; Itoh, J.; Fuchibe, K.; Akiyama, T. *J. Am. Chem. Soc.* **2007**, 129, 6756. (f) Bruvoll, M.; Hansen, T.; Uggerud, E. *J. Phys. Org. Chem.* **2007**, 20, 206. (g) Lahiri, S.; Yadav, S.; Banerjee, S.; Patil, M. P.; Sunoj, R. B. *J. Org. Chem.* **2008**, 73, 435.

(43) (a) The ρ_{BCP} values for pyrrolidine C α -H...O=C contacts in **1-TS-Ic** and **1-TS-Ia** are, respectively, 0.015 and 0.013 at the mPW1PW91/6-311G**//mPW1PW91/6-31G* level of theory. (b) These values are in similar range as noticed for standard hydrogen bonding interactions. For example, see: Koch, U.; Popelier, P. L. A. *J. Phys. Chem.* **1995**, 99, 9747. (c) See Figure S6 in the Supporting Information for more details of AIM analysis.

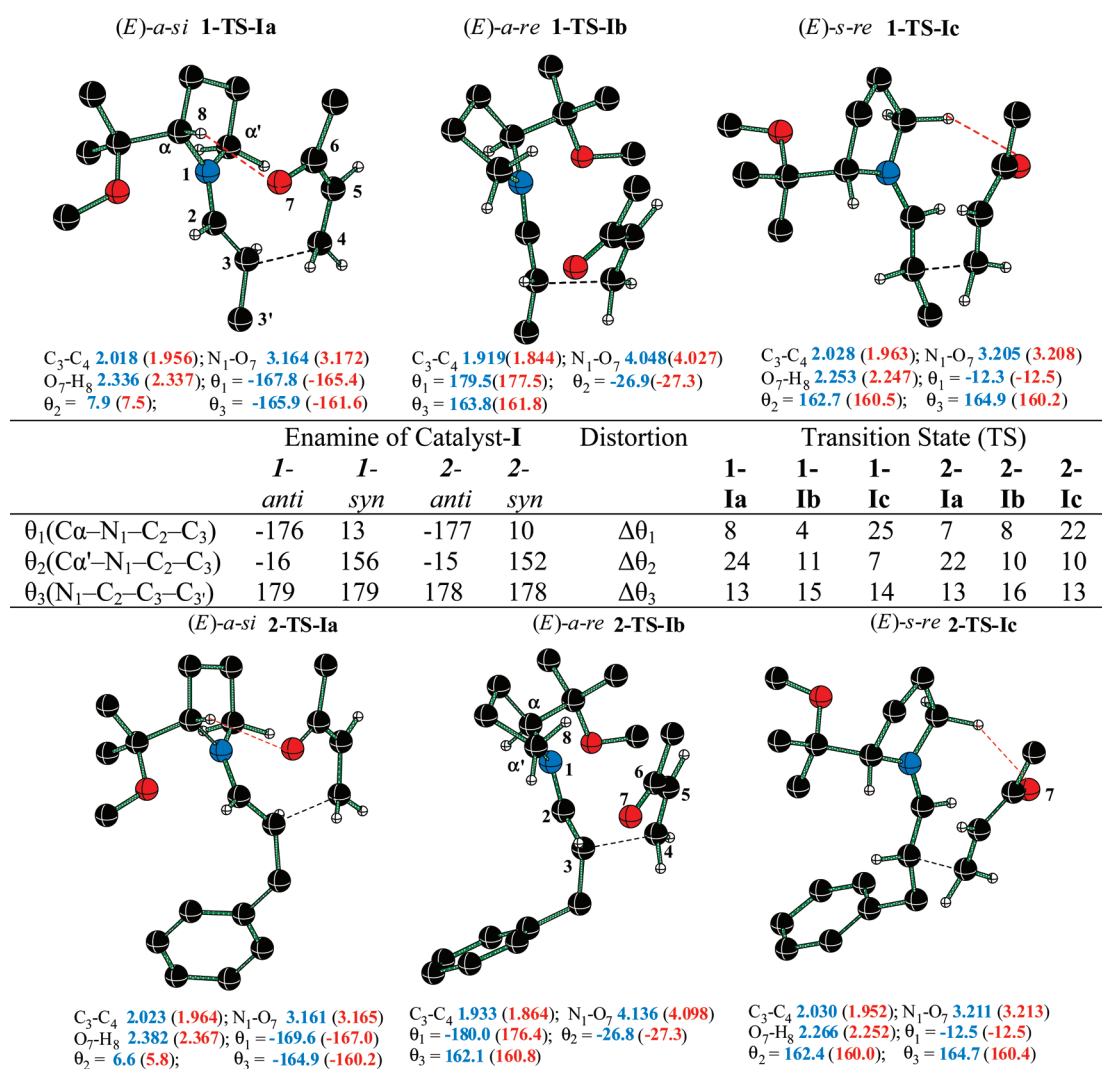


FIGURE 4. mPW1PW91/6-31G* optimized transition state geometries for the addition of enamines derived from catalyst **I** to *cis*-MVK. The values in parentheses refer to the B3LYP/6-31G* geometries. Only select hydrogen atoms are shown for sake of clarity. Angles are given in degrees and distances in Å. Atom colors: black = C, red = O, blue = N.

could be, when the hindered face of enamine adds to MVK. One such representative case, (*E*)-*a*-*re* addition, is examined. From the TS geometries **1-TS-Ib** and **2-TS-Ib**, as shown in Figure 4, it is evident that this approach would experience a destabilizing steric interaction with the α -substituent. Such interactions would severely restrict the rotameric possibilities around the incipient C–C bond.⁴⁴ Furthermore, potentially stabilizing hydrogen bonding between pyrrolidine $\text{C}\alpha'$ -hydrogen and the developing alkoxide is found to be absent in this approach. While the energy of **1-TS-Ib** and **2-TS-Ib** is higher than that of **1-TS-Ia** and **2-TS-Ia** in the case of catalyst **I**, the presence of additional stabilization effects may well change the relative energy order between these TSs. The situation could directly depend on the nature of the pyrrolidine α -substituent.

Interestingly enough the corresponding Gibbs free energy differences in the case of catalyst **II** are much smaller than that noticed for catalysts **I** and **III**. An additional hydrogen bonding interaction ($\text{O}_7\text{-H}_9$), as shown in **1-TS-IIb** and **2-**

TS-IIb (Figure 5), is noticed between MVK and the hydrogen of the diphenylmethyl substituent. However, the steric crowding offered by the bulkier α -substituent in **1-TS-IIb** and **2-TS-IIb** leads to a geometrically different mode of approach of MVK, as evident from the disposition of the substituents around the incipient C–C bond. In such an approach, potential stabilization, described in the earlier section, arising through orbital interactions in **1-TS-IIb** is expected to be ineffective.⁴⁵ As a result of the similarity in distortion of the enamine moiety and improved hydrogen bonding, **1-TS-IIb** and **2-TS-IIb** is only marginally less favored than **1-TS-IIa** and **2-TS-IIa**. The TSs with *syn* geometry of enamine, such as **1-TS-IIc** and **2-TS-IIc**, are inherently of higher energy. The above-mentioned stereo-electronic effect justifies the predicted energy order of the TSs. More importantly, the small energy differences between the competing diastereomeric TSs as noticed here could be regarded as responsible for the moderate stereoselectivity observed with catalyst **II**.

(44) It is noticed that the $\text{C}_2\text{-C}_3\text{-C}_4\text{-C}_5$ dihedral angle in **1-TS-Ib** (63.1°) is quite different from that in **1-TS-Ia** (-43.0°) and **1-TS-Ic** (42.2°).

(45) Compare with Figure 2, where stabilization of TSs through orbital interactions is provided.

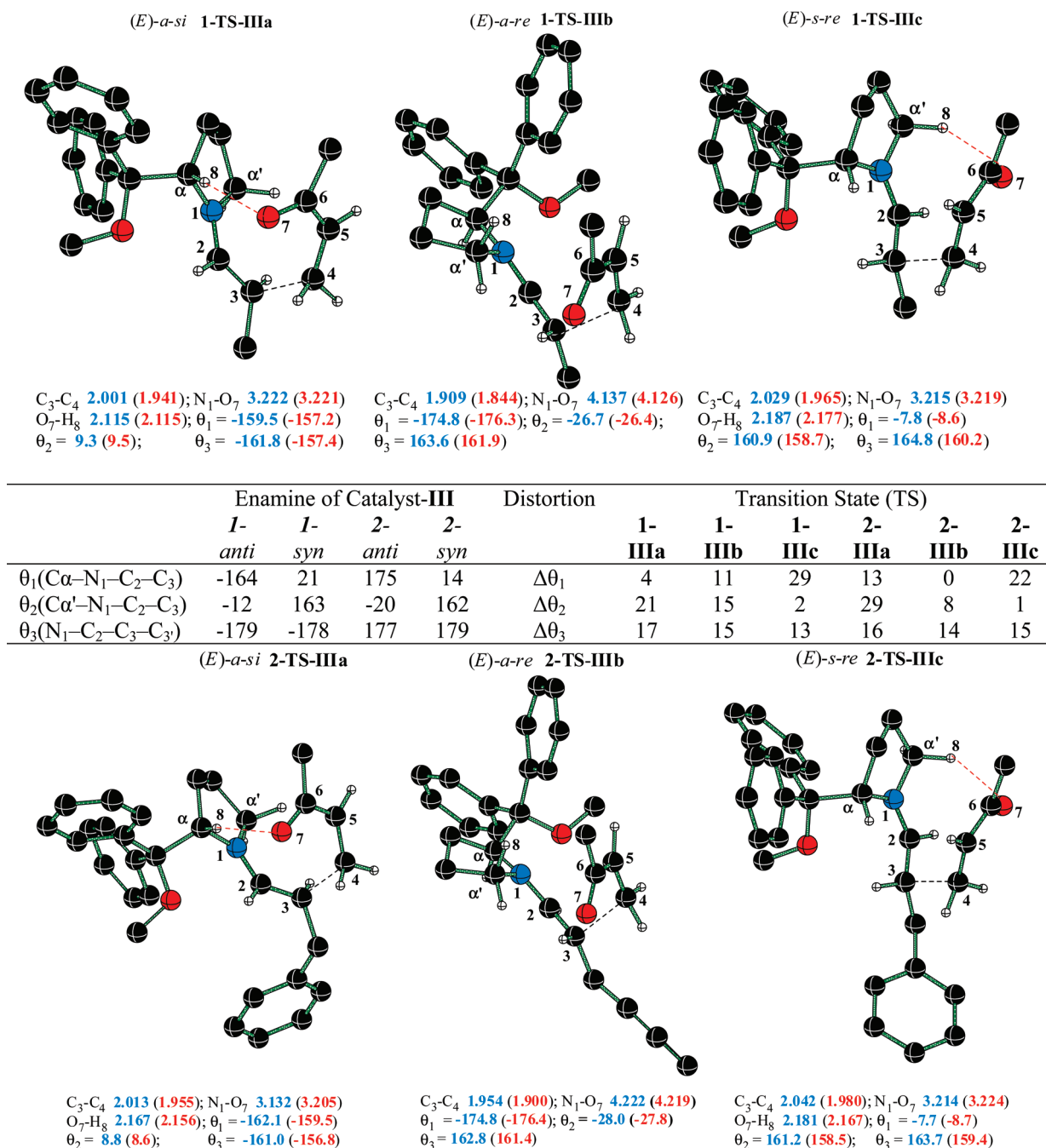


FIGURE 6. mPW1PW91/6-31G* optimized transition state geometries for the addition of enamines derived from catalyst **III** to *cis*-MVK. The values in parentheses refer to the B3LYP/6-31G* parameters. Only select hydrogen atoms are shown for sake of clarity. Angles are given in degrees and distances in Å. Atom colors: black = C, red = O, blue = N.

different stereochemical modes of addition between pyrrolidine enamine and MVK, by using catalyst **III** is provided in Figure 7. In the lowest energy TS, wherein *anti*-enamine adds to the *si* face of MVK through **1-TS-IIIa**, two favorable orbital interactions are readily evident. These are between (i) the lone pair on enamine nitrogen and the developing double bond (C5–C6) of MVK, and (ii) the enamine double bond (C2–C3) and $\pi^*_{\text{C=O}}$ of MVK (C6–O7). In the case of **1-TS-IIIb**, on the other hand, only the former type of interaction is identified. On the basis of this observation, it appears that secondary orbital interaction between the enamine and MVK

fragment should also be considered toward understanding the origin of stereoselectivity in pyrrolidine catalyzed Michael addition reactions.

In summary, it is evident that the preferred mode of approach between pyrrolidine enamines derived from propanal as well as 3-phenyl propanal to MVK would be controlled by the cumulative effect of a series of weak interactions, orbital interactions, and steric preferences. The energy separation between the diastereomeric TSs, which hold the key to stereoselectivity, can be delineated with the help of electronic structure calculations.

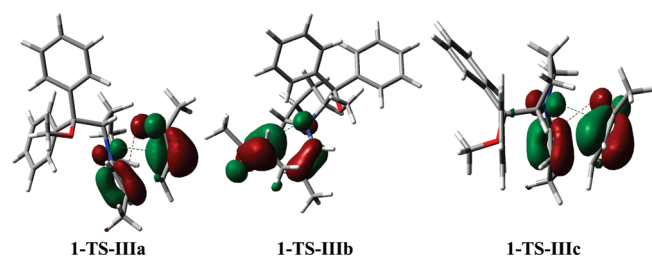


FIGURE 7. Secondary orbital interactions in the highest occupied Kohn–Sham orbital of the C–C bond formation transition states. The contours are generated at the mPW1PW91/6-311G**//mPW1PW91/6-31G* level of theory.

Conclusion

An interesting class of Michael reaction catalyzed by α -substituted pyrrolidines has been studied by using the DFT methods with an objective of gaining improved insights into the origin of stereoselectivity. Electronic structure details on the model as well as real catalytic systems have provided meaningful rationalization of available experimental observations. A number of weak interactions have been identified as responsible for the changes in stereoselectivity with respect to the nature of pyrrolidine α -substituents. A balance between stabilizing orbital interactions and hydrogen bonding contacts with destabilizing steric interactions in the

diastereomeric transition states have been found to hold the key to the observed stereoselectivity. The rationalizations on how popular organocatalysts, such as diphenylprolinol methyl ether, induces good enantioselectivity are primarily based on steric considerations. A stabilizing hydrogen bonding interaction between the developing alkoxide (of MVK) and pyrrolidine C α -H group is identified as capable of directly affecting the relative stabilization of competing transition states. Depending on the nature of the C α substituents, additional interactions with such substituents are identified as likely that could have a direct bearing on the stereochemical outcome. The results allude to possible modifications, such as the introduction of weak hydrogen bond donor or acceptor groups at the C α position, as a method to impart improved degrees of stereoselectivity.

Acknowledgment. Generous computing time from IIT Bombay computer center is gratefully acknowledged. A.K. S. acknowledges CSIR-New Delhi for a Senior Research Fellowship.

Supporting Information Available: Optimized geometries for all stationary points obtained at different levels of theory, total electronic energies, bond order, natural charges, AIM analyses, and IRC plots for transition states. This material is available free of charge via the Internet at <http://pubs.acs.org>.